공학석사학위논문

고정밀 구조응답 예측을 위한 Bezier 사면체 요소 기반 isogeometric 해석 개발

Development of an Isogeometric analysis based on Bezier tetrahedral element for high-precision structural prediction

2023 년 2 월

서울대학교 대학원

항공우주공학과

송 동 현

고정밀 구조응답 예측을 위한 Bezier 사면체 요소 기반 isogeometric 해석 개발

Development of an Isogeometric analysis based on Bezier tetrahedral element for high-precision structural prediction

지도교수 신 상 준

이 논문을 공학석사 학위논문으로 제출함

2022 년 10 월

서울대학교 대학원

기계항공공학부

송 동 현

송동현의 공학석사 학위논문을 인준함

2022 년 12 월

위 원 장	**조선호**	**(인)**
부위원장	**신상준**	**(인)**
위 원	**김도년**	**(인)**

Abstract

Development of an Isogeometric analysis based on Bezier tetrahedral element for high-precision structural prediction

Dong-Hyeon Song

Department of Aerospace Engineering

The Graduate School

Seoul National University

Precise prediction is one of the essential components in the design stage of the various engineering objects. Certain curved configuration of it may induce severe discretization inaccuracy when it is analyzed by the conventional finite element method (FEM). Meanwhile, an isogeometric analysis (IGA) that combines the computer-aided design (CAD) and FEM is capable of more precise numerical computation when compared against FEM. It is due to that the exact geometry is represented identically as CAD does and high inter-element continuity of the basis function is maintained. Actually, prediction of more precise numerical results has been verified on many engineering areas such as fluids, solids, and electromagnetics. However, application of the IGA for a complicated three-dimensional object has not been successful. The main reasons of that are NURBS basis function which defined as tensor product, and Boundary representation (B-rep) of CAD software. Because

of the NURBS defined as tensor product, multi-patch is required for representing complicated geometry. Furthermore, B-rep of CAD software means that the three-dimensional solid objects is represented using only the bounding surfaces without the inner volumetric information. To overcome such limitation, many alternatives have been suggested including the method using Bezier element. The present method presented in this thesis is based on such idea.

In this thesis, the three-dimensional solid geometry will be inner volumetric parameterized by FE discretization. Then, Bernstein-Bezier discretization that represents the curved surface with quite smaller geometric discrepancy will be obtained by the surface reconstruction. Then, an approximate C^1 Bezier basis function will be obtained by the linear combination of C^0 Bezier basis function based on the continuity coefficients. The remaining analysis will be carried out using the C^1 Bezier basis function. For the computational efficiency, the macro element splitting technique that will split a single macro tetrahedron into multiple micro tetrahedrons will be utilized. Finally, an approximate C^1 Bezier basis function will be applied to the various curved solid objects that include the realistic geometry. Unlike the previous method using 5th order Bezier tetrahedral element, present method utilizes a conventional 2nd order element. Therefore, more improved applicability for arbitrary geometry can be obtained by applying the graph algorithm in pre-processing with the conventional element. Also, by utilizing the commercial FEM software, there is no requirement for combining the inconsistency which occurred on the intersection of NURBS surfaces as in the previous work.

The verification of the present method will be accomplished by comparing the discrepancy on von-Mises stress by the present prediction against those by the traditional FEM. Additionally, NASA Rotor 67 blade configuration is selected for verifying the improved applicability of the present method.

Keywords: Isogeometric analysis, Finite element method, Tetrahedral Bezier spline, Bezier tetrahedron, Macro element split, C^1 continuity condition, FE discretization

Student Number: 2021-27453

Contents

Page

List of Tables

Page

List of Figures

Page

List of Symbols

Symbols	Meaning
N, M	B-spline basis function
R	NURBS basis function
B	Bezier basis function
P	Control point
w	Weight of control point
$\xi,\ \eta$	Parametric point
λ	Barycentric coordinate
$\mathcal{M}$	MDS
A	Continuity matrix
$c, \tilde{c}$	B-coefficient
d	Order of basis function
T	Bezier tetrahedron
b_f	Body force
t	Traction force
ϕ	C^0 basis function
ψ	C^1 basis function
V	Total volume of the domain
Ω	Total domain
Γ_t	Surface imposed by Neumann boundary condition

Γ_u	Surface imposed by Dirichlet boundary condition
K_{MDS}	Stiffness matrix defined on MDS

Chpater 1

Introduction

1.1 Background and Motivation

Turbine blade, of which one of the complicated mechanical geometries, is usually operated in harsh environments. The high temperature and high speed-rotation may lead to the blade failure, and therefore precise prediction in its design process will be crucial.

Certain curved configuration of it may induce severe discretization inaccuracy when it is analyzed by the conventional FEM. One of the alternatives for alleviation of such inaccuracy, isogeometric analysis (IGA) has been proposed as a means to combine the traditional computer-aided design (CAD) along with the FEM [1]. It utilizes the same basis function as that CAD uses, non-uniform rational B-spline (NURBS), to describe both the geometry and physical quantities in the field. The detailed CAD geometry reduces the approximation discrepancy induced by FE polygonal discretization. And because the NURBS basis function has higher inter-element continuity, a more precise numerical behavior may be obtained. IGA has been successfully applied in many engineering fields, such as structural vibration [2, 3], fluids [4], electromagnetics [5], shell analysis [6], and fluid-structure interaction analysis [7]. Especially in the structural analysis, precise and continuous stress computation will be conducted because of its higher-order inter-element continuity

originated by NURBS basis function. Similarly, IGA is known to provide a more precise solution than the traditional FEM does regarding the multiple curved surfaces. The main reason of that is the representation of curved configuration more exactly than FE polygon. However, application of NURBS-based IGA to various engineering geometries will not be straightforward because there does not exist an appropriate preprocessor. It is due to that a multi-patch object will be required for representing the complicated geometry because of the NURBS which expressed as a tensor product. In most of CAD software, three-dimensional solid object is represented as boundary-representation (B-rep) that represents only the boundary surface of the object. Therefore, it is not suitable for numerical analysis because of the absence of the inner volumetric information for the analysis configuration.

To overcome such limitation, quite a lot of researches have been executed to find an advanced solution methodology. Aigner proposed a swept volume parameterization for IGA [8], while generating an inner volumetric parameterization from the given boundary condition and guiding curves. Kim [9] proposed IGA for the trimmed CAD surface that used the triangular or quadrilateral elements with only one trimmed edge by decomposing the surface. Jaxon and Xia [10, 11] proposed IGA on the discretized field, where the triangular and tetrahedral Bezier elements were used for an inner volumetric parameterization. Kadapa [12] proposed the quadratic C^0 Bezier mesh generation technique for a unified pre-processing framework. Also, an idea of using the other splines such as T-splines [13] and U-splines [13] instead of NURBS of Bezier spline for the solid IGA was proposed. Other than those, a

scaled boundary IGA which utilized NURBS information of B-rep of CAD and parameterized the inner volume by a radial scaling factor was proposed by Chasapi [15].

Similarly, there have been several attempts that employed IGA for the turbine blade, which contained multiple curved surfaces. Hsu [16] generated a CAD result which was IGA-suitable by a parametric modeling on a turbine blade while using Grasshopper, an add-on program by Rhinoceros CAD software, Inc. Bazilevs [17] analyzed the fluid and structural vibration by using IGA on the turbine blade used for Black Hawk and Apache helicopters by using NURBS mesh generation.

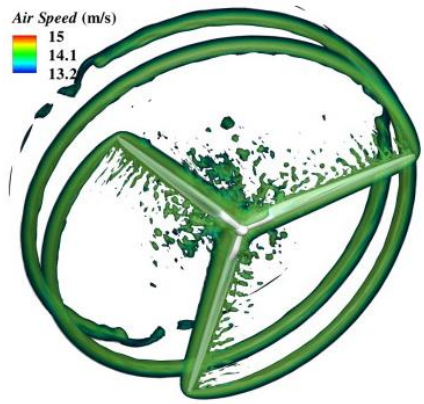

(a)fluids

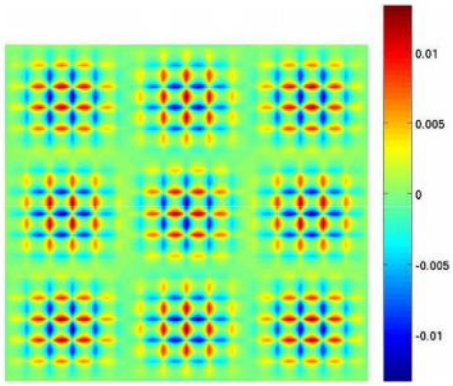

(b) electromagnetics

Fig. 1.1 Application of NURBS-based IGA for various fields

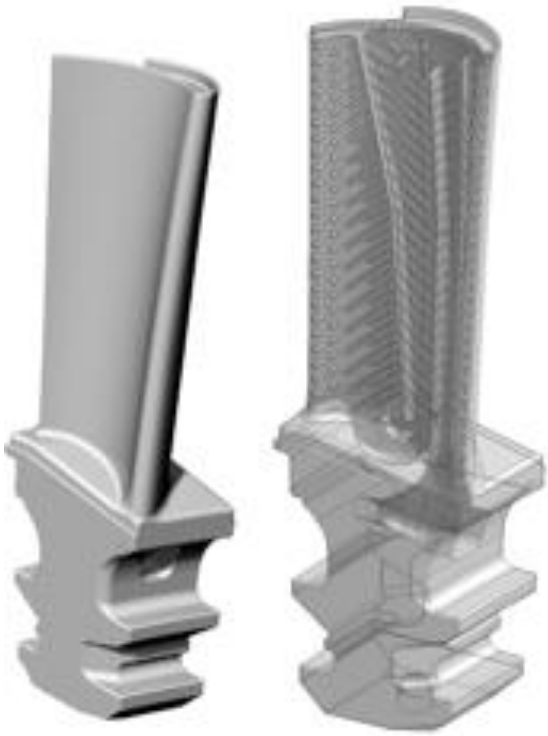

Fig. 1.2 Turbine blade which contains multiple curved surfaces [26]

Fig. 1.3 NURBS basis function [1]

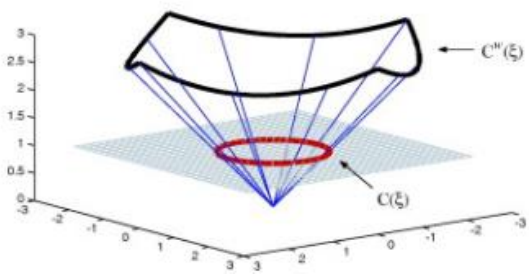

Fig. 1.4 Comparison between B-spline and NURBS [1]

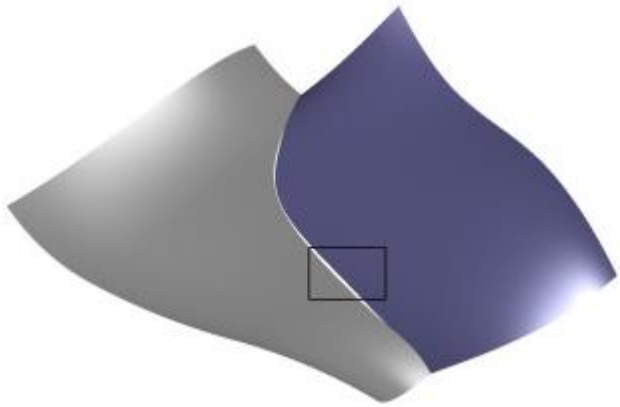

Fig. 1.5 Difference of NURBS surfaces occurred on the intersection [11]

1.2 Research objective

The present method is inspired by IGA based on Bezier tetrahedra for more precise structural analysis. Compared with the previous work, the present framework is more applicable to any arbitrary geometry by using the conventional lower order tetrahedron and unified preprocessing with a graph algorithm. Furthermore, the combining process for the different NURBS surface occurred on the intersections of tetrahedron is not required. By using the commercial FE preprocessing software, the different NURBS surface is combined already.

The inner parameterized FE polygon is transformed into the Bezier elements by using the surface reconstruction for reducing the geometric discrepancy. However, the reconstructed element is not a exact geometry. It's because Bezier spline corresponds to the knot span of B-spline, which is the non-rational form of NURBS. Despite, if single curved surface represented with multiple Bezier surface than the geometry discrepancy will be reduced significantly. Also, by applying the additional continuity condition to C^0 Bezier basis, a more continuous basis will be obtained. Applying the continuity condition is conducting Hermite interpolation for intersection of all tetrahedrons. As a result, the features of NURBS-based IGA for precise analysis will be implemented in the present method.

To obtain an inner volumetric parameterization of a solid object, finite element (FE) discretization using a tetrahedral element will be performed by the commercial software ANSYS. The resulting tetrahedral element will be converted into a

quadratic C^0 Bezier element by the surface reconstruction technique. The resulting Bezier element will represent a curved geometry with significantly decreased geometric discrepancy than that by a traditional FE polygon. Especially, more Bezier element utilized for representing the single CAD geometry. Then, an approximate C^1 Bezier basis function will be obtained by a linear combination of C^0 Bezier basis function and continuity coefficients. The continuity coefficients will be obtained by applying the relevant condition to all C^0 Bezier tetrahedrons. In other words, Hermite interpolation will be applied to all the intersections on each tetrahedron. When applying the continuity condition, the macro element spliting technique will be used for efficiency, and a minimal determining set (MDS), which represents all the domain points, be defined. The resulting MDS and approximate C^1 basis function which is defined only on MDS will be used for the remaining analysis. A complete framework of TBS-based IGA will be constructed and carried out on the curved solid object. Then the present method will be verified by comparing its results against those by the analytic solution and FEM.

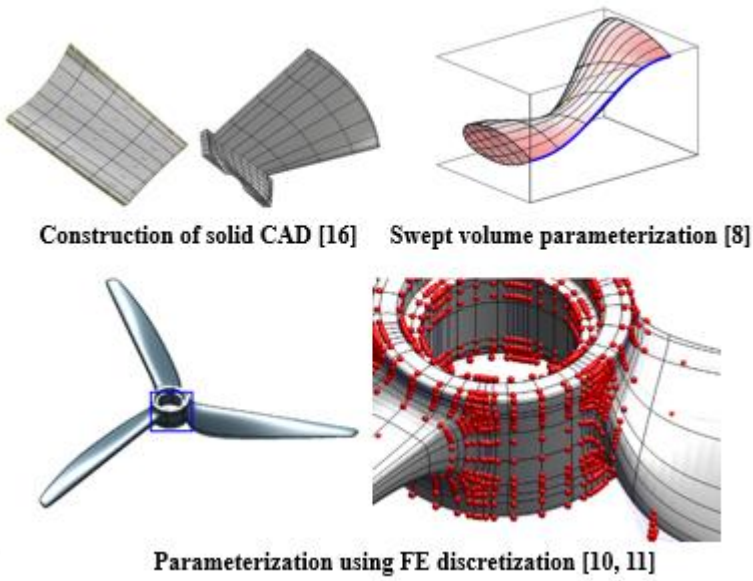

Fig. 1.6 Alternatives for three-dimensional solid IGA

1.3 Thesis overview

In this thesis, the framework of tetrahedral Bezier spline (TBS)- based IGA will be presented, and attempted on three-dimensional solid object including the turbine blade geometry. The proposed method is characterized by the summaries as follows:

1. For precise numerical solution, the proposed methodology implements the features of NURBS-based IGA, of which the spline-based geometric representation and improved continuity of basis function.

2. For an application of the present method to three-dimensional solid object, FE discretization will be utilized for an inner volumetric parameterization.

3. When compared against the previous work [10, 11], the present method will improve the applicability for an arbitrary solid object by using the conventional tetrahedral element, and a graph preprocessing algorithm.
4. For the verification of the present method can calculate more precise numerical solution than traditional FEM, curved solid geometry is selected.
5. For the verification of the improved applicability of the present method, NASA Rotor 67 is selected.

Chpater 2

NURBS and Bernstein-Bezier Technique

2.1 NURBS

CAD geometry is usually defined by NURBS-expressed boundary which is described by a linear combination between the control point and basis function at a few parametric locations. NURBS basis is defined by the control point, weight, and knot vectors [18]. According to Cox-deBoor recursion formula, the p-th order B-spline basis function is defined as in Eqs. (2.1) and (2.2). The p-th order NURBS basis functions are defined as Eq. (2.3).

$$\boldsymbol{N_{i,0}(\xi)} = \begin{cases} \mathbf{1} & \boldsymbol{if\ \xi_i \le \xi < \xi_{i+1}} \\ \mathbf{0} & \boldsymbol{otherwise} \end{cases} \tag{2.1}$$

$$\boldsymbol{N_{i,0}(\xi)} = \frac{\boldsymbol{\xi - \xi_i}}{\boldsymbol{\xi_{i+p} - \xi_i}} \boldsymbol{N_{i,p-1}(\xi)} + \frac{\boldsymbol{\xi_{i+p+1} - \xi}}{\boldsymbol{\xi_{i+p+1} - \xi_{i+1}}} \boldsymbol{N_{i+1,p-1}(\xi)} \tag{2.2}$$

$$\boldsymbol{R_{i,j}^{p,q}(\xi,\eta)} = \frac{\boldsymbol{N_{i,p}(\xi) M_{j,q}(\eta) w_{i,j}}}{\boldsymbol{\sum_{i=1}^{n+p+1} \sum_{j=1}^{m+q+1} N_{i,p}(\xi) M_{j,q}(\eta) w_{i,j}}} \tag{2.3}$$

where n, m is the number of the basis functions, w is the weight of the control point and ξ, η indicate the parametric coordinate. ξ_i is the i-th knot vector where $\Xi = \{\xi_1, \xi_2, \cdots, \xi_{n+p+1}\}$ and η_j is the j-th knot vector where $\Phi = \{\eta_1, \eta_2, \cdots, \eta_{m+q+1}\}$. $N_{i,p}$ and $M_{j,q}$ are the p-th and q-th order B-spline basis function,

respectively. $R_{i,j}^{p,q}$ is NURBS basis function defined by $N_{i,p}$ and $M_{j,q}$.

Then, NURBS surface $S^{nurbs}(\xi, \eta)$ can be defined as the linear combination of the basis function and control points as in Eq. (2.4).

$$\boldsymbol{S^{nurbs}}(\boldsymbol{\xi}, \boldsymbol{\eta}) = \sum_{i=1}^{n} \sum_{j=1}^{m} R_{i,j}^{p,q} P_{i,j} \,. \tag{2.4}$$

2.2 Bernstein-Bezier technique

2.2.1 Bezier surface

Bezier surface corresponds to each knot span of B-spline surface, the same as the non-rational NURBS surface. Bezier surface is defined by a linear combination of Bernstein basis functions and control points. The d-th order Bernstein polynomial is defined as in Eq. (2.5). The d-th order Bezier surface is defined as in Eq. (2.6).

$$\boldsymbol{B_{i,d}(\xi) = \frac{d!}{i!\,(d-i)!}\xi^{i}(1-\xi)^{d-i}, \quad \xi \in [0,1].} \tag{2.5}$$

$$\boldsymbol{S^{bezier}(\xi,\eta) = \sum_{i=1}^{k+1}\sum_{j=1}^{l+1} B_{i,k}(\xi)B_{j,l}(\eta)\,K_{i,j}\,.} \tag{2.6}$$

where k, l are the degree of Bernstein basis, and ξ, η indicate the parametric coordinate, respectively. $B_{i,d}$ is the d-th order Bernstein basis function, $K_{i,j}$ is the control point, and $S^{bezier}(\xi, \eta)$ is Bezier surface at parametric location.

2.2.2 Bezier tetrahedron

All the points located at the inner side of the tetrahedron may be represented by using the barycentric coordinate $\lambda = [\lambda_1, \lambda_2, \lambda_3, \lambda_4]$ which is rewritten in terms of the volume of the tetrahedron $T = \{v_1, v_2, v_3, v_4\}$ as shown in Eqs. (2.7) and (2.8).

$$\boldsymbol{\lambda_i = \frac{V_i}{V}.} \tag{2.7}$$

$$\boldsymbol{P}(\boldsymbol{\lambda}) = \boldsymbol{\lambda_1 v_1} + \boldsymbol{\lambda_2 v_2} + \boldsymbol{\lambda_3 v_3} + \boldsymbol{\lambda_4 v_4}. \tag{2.8}$$

Bernstein basis function will be defined using the barycentric coordinate for a tetrahedron in the parent space. The d-th order Bernstein basis is defined as shown in Eq. (2.9).

$$\boldsymbol{B^d_{ijkl}}(\boldsymbol{\lambda}) = \frac{\boldsymbol{d}!}{\boldsymbol{i}!\,\boldsymbol{j}!\,\boldsymbol{k}!\,\boldsymbol{l}!}\boldsymbol{\lambda_1^i \lambda_2^j \lambda_3^k \lambda_4^l}, \quad \boldsymbol{i + j + k + l = d}. \tag{2.9}$$

Then Bezier tetrahedron in the physical space will be represented a linear combination of Bernstein basis and control point as Eq. (2.10).

$$\boldsymbol{T}(\boldsymbol{\lambda}) = \sum_{\boldsymbol{i+j+k+l=p}} \boldsymbol{B^d_{ijkl}}(\boldsymbol{\lambda})\boldsymbol{P_{ijkl}}\,. \tag{2.10}$$

where P_{ijkl} is the control point in the physical space.

2.2.3 Derivatives of a polynomial in B-form

The directional derivative at point v with respect to the direction u is defined as shown in Eq. (2.11), and the direction vector u is defined using $a = (a_1, a_2, a_3, a_4)$ in terms of the barycentric coordinate. The quantity, $c^{(1)}_{ijkl}(a)$ are obtained from the first step of *de Casteljau* algorithm as shown in Eq. (2.12).

$$\boldsymbol{D_u p}(\boldsymbol{v}) = \boldsymbol{d} \sum_{\boldsymbol{i+j+k+l=d}} \boldsymbol{c^{(1)}_{ijkl}}(\boldsymbol{a})\boldsymbol{B^{d-1}_{ijkl}}(\boldsymbol{v})\,. \tag{2.11}$$

$$c_{ijkl}^{(1)}(a) = c_{i+1,j,k,l}a_1 + c_{i,j+1,k,l}a_2 + c_{i,j,k+1,l}a_3 + c_{i,j,k,l+1}a_4. \tag{2.11}$$

$$i + j + k + l = d - 1$$

where $c_{i,j,k,l}$ is the control point, and B_{ijkl}^{d} is the d-th order Bezier basis function.

Chpater 3

TBS-based isogeometric analysis

3.1 Framework of TBS-based IGA

For the convenience, the complete framework of TBS-based IGA is depicted using a two-dimensional curved geometry example as shown in Fig. 3.1. Diminishing the geometric discrepancy and utilizing a high inter-element continuous shape function are the main features of NURBS-based IGA for an accurate numerical analysis. To implement those features in the present method, pre-processing techniques such as surface reconstruction and applying continuity condition by using macro element split will be used.

First, the surface reconstruction will be attempted. Using the commercial FEM software, CAD geometry, represented as B-rep, will become inner parameterized by using FE discretization that contains the geometrical discrepancy on the curved boundary. To reduce it, FE tetrahedral elements will be converted into C^0 Bezier tetrahedral elements by the surface reconstruction process. In the process, control points of each Bezier element will be obtained by using the definition of TBS spline with the physical coordinate from FEM software. However, the reconstructed Bezier element represents the exact geometry as the NURBS. By representing with multiple Bezier elements for single curved surface, it will be resolved. The converted Bezier elements will exhibit significantly reduced geometric discrepancy than FE

tetrahedral elements do when representing the curved geometry. In this process, input information for the in-house code is only from the commercial FEM software. Because there is no requirement of the NURBS information for each surfaces, and the graph algorithm is utilized for finding the element located on boundary.

Second, the continuity condition is applied to obtain C^1 basis function. In general, the construction of C^1 basis requires over the 9th-order tetrahedral element. For computationally efficient analysis, approximate C^1 basis could be constructed using the lower-order tetrahedral element by utilizing the macro element split. In the splitting element, split condition for macro edge is violated for the alleviation of the geometric constraint. By doing that, the present method can be applied to complicated geometry such as curve-dominant geometry. However, the C^1 continuity is violated on the midpoint of macro edge. Consequently, the approximate C^1 basis, of which not exact C^1 on the macro edge is constructed. After that, the minimal determining set (MDS) will be defined by applying the continuity condition on all of C^0 Bezier elements. By The approximate C^1 Bezier basis is defined on MDS by a linear combination of C^0 Bezier basis and continuity coefficients, and utilize it for representing the overall physical field.

By conducting the above pre-processing process, the features of the NURBS-based IGA for precise numerical analysis can be implemented. As mentioned earlier, this process requires only the information from the commercial FEM software as the input information by utilizing the graph algorithm. Such unified preprocessing has advantage of improved applicability for arbitrary complicated geometry.

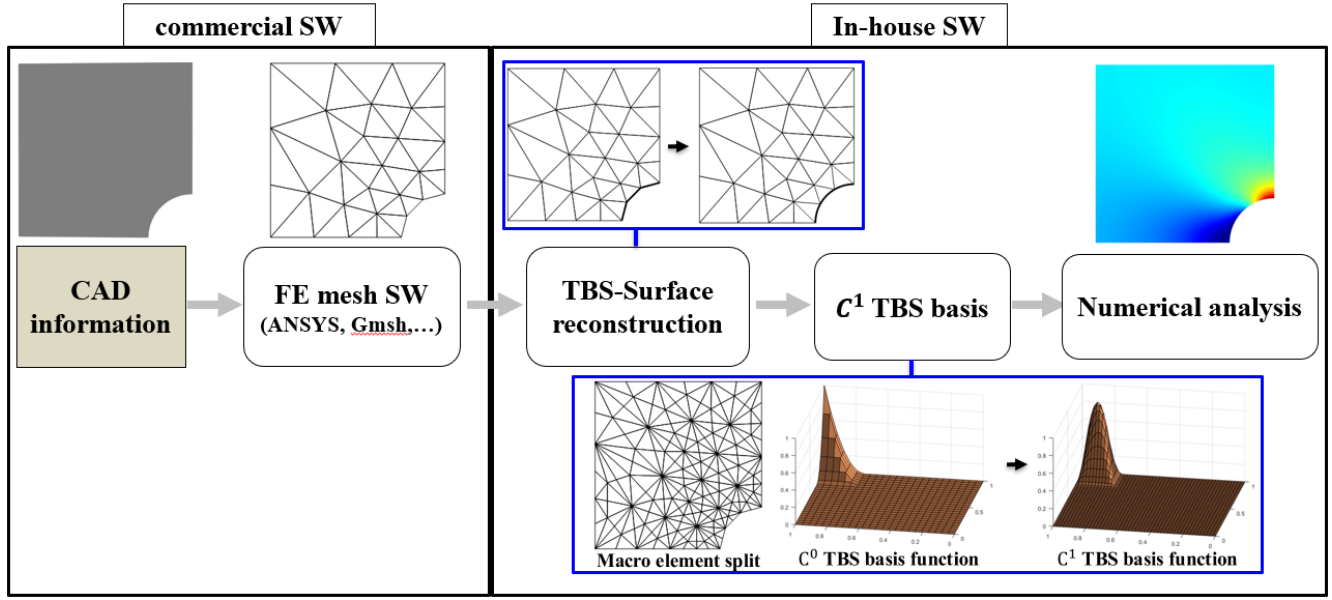

Fig. 3.1 Framework of the present method

After pre-processing, the numerical analysis may be conducted by utilizing the physical field with a reduced geometrical discrepancy and the approximate C^1 Bezier basis function defined on the MDS. Entire analysis procedures are similar to the traditional FE formulation except that the solution is obtained on MDS points. In other words, the matrix of properties such as the stiffness is constructed only using the MDS. Figure 3.2 illustrates the analysis procedure of the present method. First, because approximate C^1 Bezier basis function is defined on the parametric space, physical control points and boundary condition will be projected onto the linearized parametric space. Then, the analysis will be conducted on MDS. Finally, calculated parametric field will be projected onto the physical space. Consequently, the numerical analysis for physical space that represents that contains highly reduced geometric discrepancy is conducted.

The comparison of the entire analysis procedure for the present method with NURBS-based IGA and traditional FEM is illustrated in Fig 3.3 using two-dimensional example geometry. The formulation for all method is same except the analysis is conducted on the control point in NURBs-based IGA, node in the FEM, and MDS in the present method. In NURBS-based IGA, the NURBS basis function is defined on the parametric space represented as rectangle. Then, the numerical solution will be calculated on physical space directly because it utilizes the same geometry representation as CAD does. In traditional FEM, after the CAD geometry discretization by FE polygon, nodal displacement will be calculated. For stress calculation, it requires additional stress recovery technique such as extrapolation.

Meanwhile, the present method utilizes the FE discretized geometry as parametric space. The numerical solution will be calculated on parametric space, of which the approximate C^1 basis function is defined. Finally, the solution will be projected onto the physical space.

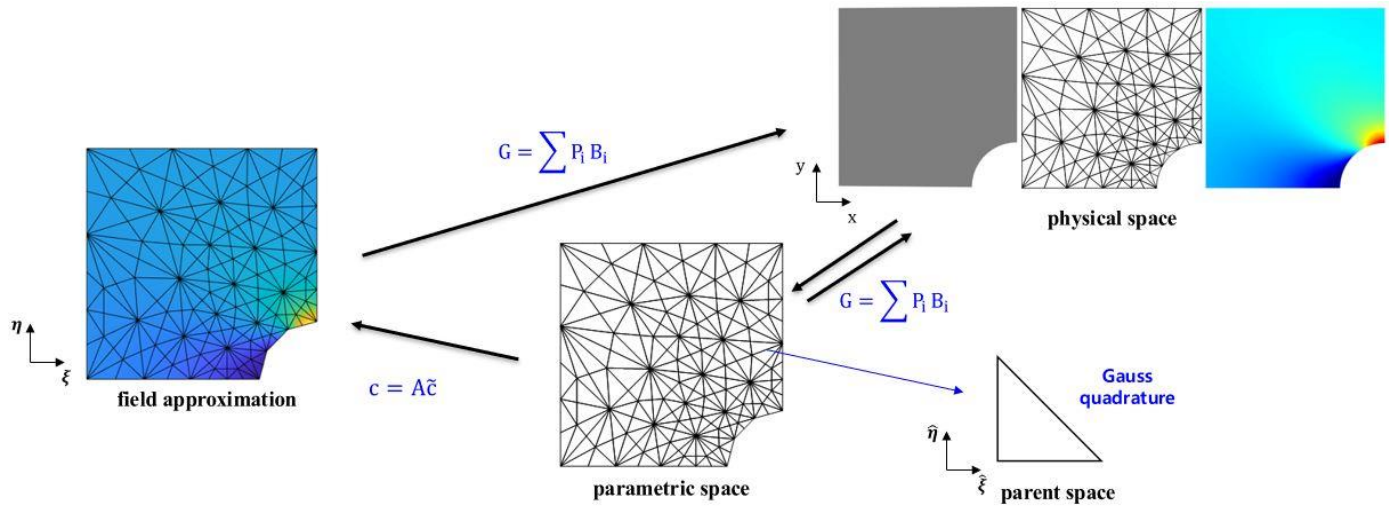

Fig. 3.2 Present analysis procedure

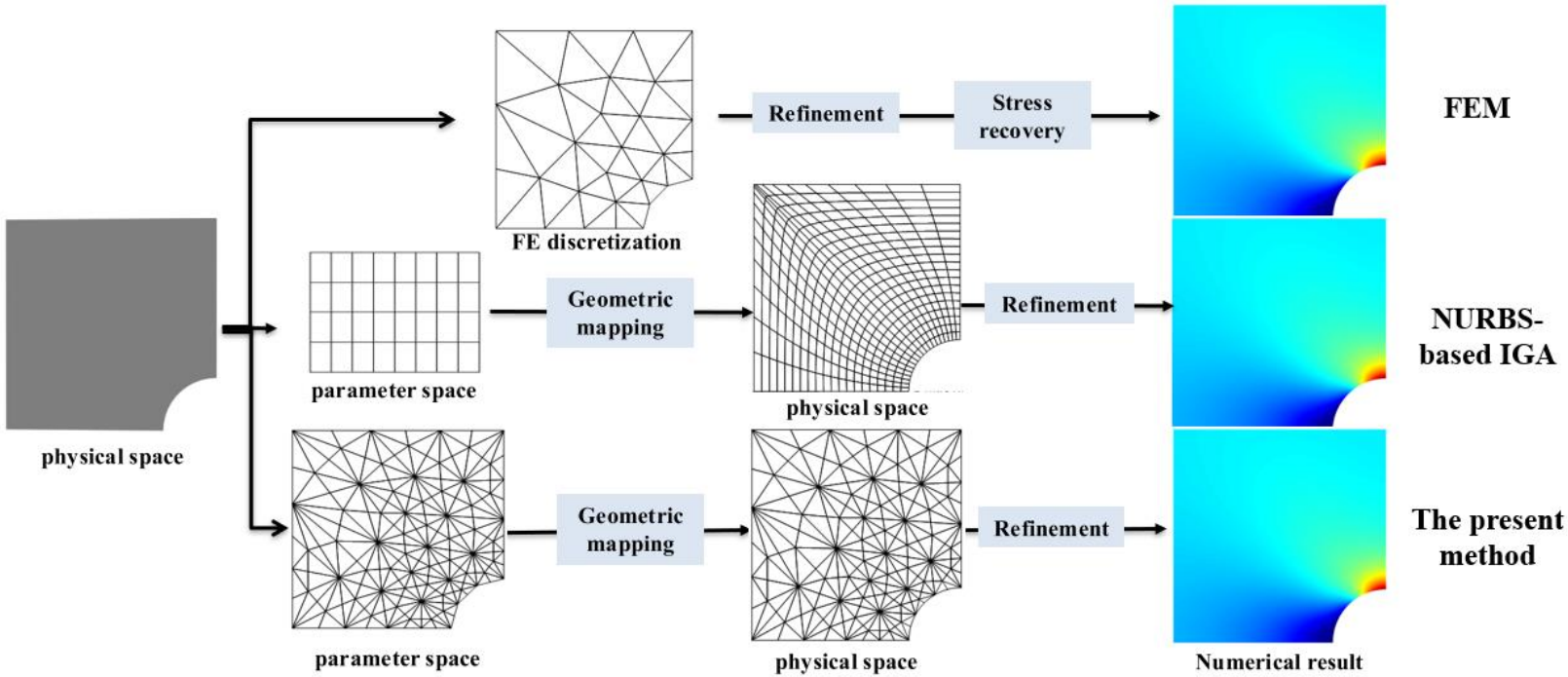

Fig. 3.3 Comparison of the analysis procedures

3.2 Surface reconstruction

As expressed in the previous section, CAD represents a solid as B-rep without an inner volumetric information, and it is necessary to create an inner volumetric parameterization for the numerical analysis. In this paper, ANSYS, a FEM software, will be used for FE discretization with a conventional 2nd order tetrahedral element.

First, FE discretization by using the tetrahedral mesh will be performed to parameterize the interior of the domain. However, the surface of the FE discretized geometry is represented by using the polygonal mesh. Thus, the surface reconstruction is required to represent the curved surface with the reduced geometric discrepancy.

Second, it is assumed that all the tetrahedral elements will be Bezier elements, and then the relationship that the physical points obtained from FEM SW will be the same as Bezier surface at the boundary parametric space. Therefore, the linear combination of Bezier basis ($\boldsymbol{B}$) at the parametric coordinate ($\hat{\boldsymbol{\lambda}}$) and Bezier control points ($\boldsymbol{P^b}$) will be the same as the physical points of CAD ($\boldsymbol{x}|_{\boldsymbol{phy}}$). For one tetrahedron, this relation will be described as Eq. (3.1), in a matrix form as in Eqs. (3.2) and (3.3) and the matrices of basis and control point are described as Eqs. (3.4) and (3.5). Figure 3.4 describe the entire from FE polygonal element to Bezier element tor two-dimensional curved geometry.

$$\boldsymbol{x}|_{\boldsymbol{phy}} = \sum_{\boldsymbol{i=1}}^{\boldsymbol{n_f}} \boldsymbol{B_{i,p}}(\hat{\boldsymbol{\lambda}})\boldsymbol{P_i^b}. \tag{3.1}$$

$$\boldsymbol{x}|_{\boldsymbol{phy}} = \boldsymbol{B}(\hat{\boldsymbol{\lambda}})\boldsymbol{P}^{\boldsymbol{b}}. \tag{3.2}$$

$$\boldsymbol{P}^{\boldsymbol{b}} = \boldsymbol{B}^{-\boldsymbol{1}}(\hat{\boldsymbol{\lambda}})\boldsymbol{P}^{\boldsymbol{p}}. \tag{3.3}$$

$$\boldsymbol{B}(\hat{\boldsymbol{\lambda}}) = \begin{bmatrix} \boldsymbol{B}_{\boldsymbol{1},\boldsymbol{p}}(\hat{\boldsymbol{\lambda}}_{\boldsymbol{1}}) & \boldsymbol{B}_{\boldsymbol{2},\boldsymbol{p}}(\hat{\boldsymbol{\lambda}}_{\boldsymbol{1}}) & \cdots & \boldsymbol{B}_{\boldsymbol{n_f},\boldsymbol{p}}(\hat{\boldsymbol{\lambda}}_{\boldsymbol{1}}) \\ & & \vdots & \\ \boldsymbol{B}_{\boldsymbol{1},\boldsymbol{p}}\left(\hat{\boldsymbol{\lambda}}_{\boldsymbol{n_f}}\right) & \boldsymbol{B}_{\boldsymbol{2},\boldsymbol{p}}\left(\hat{\boldsymbol{\lambda}}_{\boldsymbol{n_f}}\right) & \cdots & \boldsymbol{B}_{\boldsymbol{n_f},\boldsymbol{p}}\left(\hat{\boldsymbol{\lambda}}_{\boldsymbol{n_f}}\right) \end{bmatrix}. \tag{3.4}$$

$$\mathbf{P}^{\boldsymbol{p}} = \begin{bmatrix} \boldsymbol{x}_{\boldsymbol{1}}^{\boldsymbol{phy}} \\ \boldsymbol{x}_{\boldsymbol{2}}^{\boldsymbol{phy}} \\ \vdots \\ \boldsymbol{x}_{\boldsymbol{n_s}}^{\boldsymbol{phy}} \end{bmatrix}, \ \mathbf{P}^{\mathbf{b}} = \begin{bmatrix} \boldsymbol{P}_{\boldsymbol{1}}^{\boldsymbol{b}} \\ \boldsymbol{P}_{\boldsymbol{2}}^{\boldsymbol{b}} \\ \vdots \\ \boldsymbol{P}_{\boldsymbol{n_s}}^{\boldsymbol{b}} \end{bmatrix}. \tag{3.5}$$

Where n_f and n_s are number of boundary elements and number of nodes per each face, respectively.

Although Bezier extraction [20] and Bezier projection [21] may be used for the surface reconstruction, these will be the local operators and there is a constraint that Bezier element face should be located in one NURBS knot span. Therefore, there exists a difficulty in applying those to any FE discretized domain. However, utilizing the definition of Bezier surface, presented in [12], becomes free from such constraints. In addition, the present process may be conducted only by the conventional FE preprocess software because there exists no requirement for NURBS information for each surface. Such unified preprocess is achieved by utilizing a graph algorithm for searching the elements that located on the boundary surface. As a result, the present method has an advantage of enlarged applicability for an arbitrary complicated geometry. Despite the above-mentioned advantages, the

reconstructed surface may not represent an exact CAD geometry with the weight of the control points between zero and unity, the weight of the reconstructed surface for all the control points will be a unity. However, when the single surface is represented by multiple number of the non-rational surfaces, the geometric discrepancy will become small against the rational surface. Regarding the visualization of the discrepancy in each situation, FE polygon, non-rational TBS, and NURBS curve are shown in Fig. 3.5.

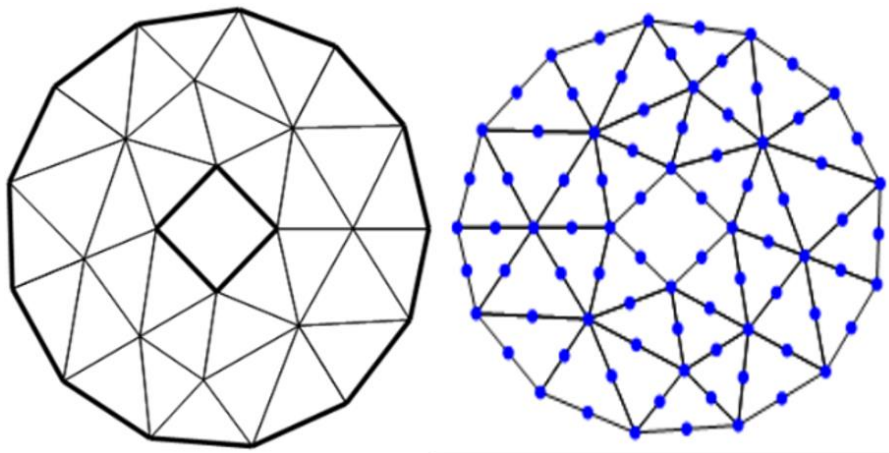

(a) FE triangular element

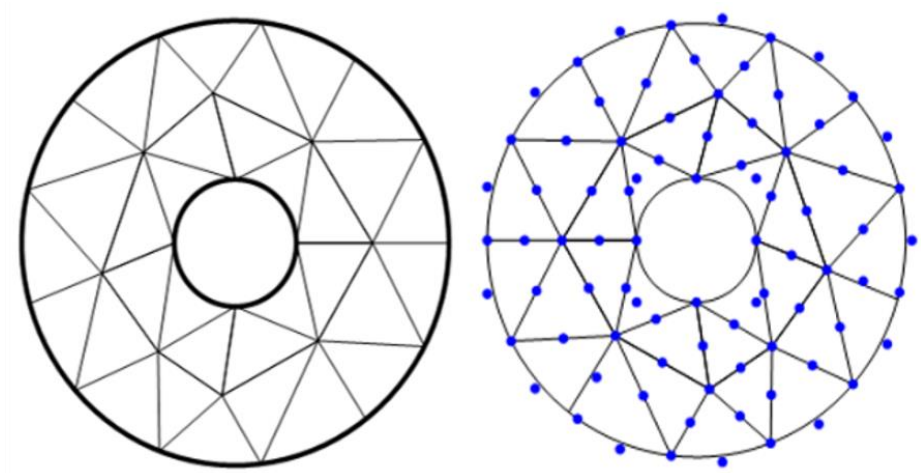

(b) C^0 Bezier element

Fig. 3.4 Surface reconstruction of a two-dimensional object

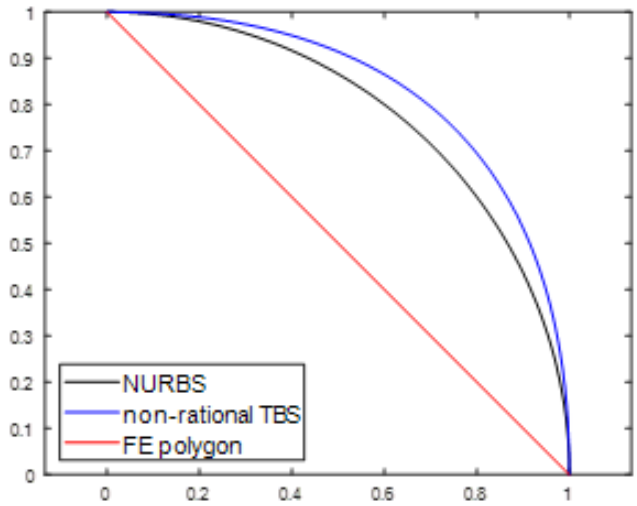

(a) Number of the curves = 1

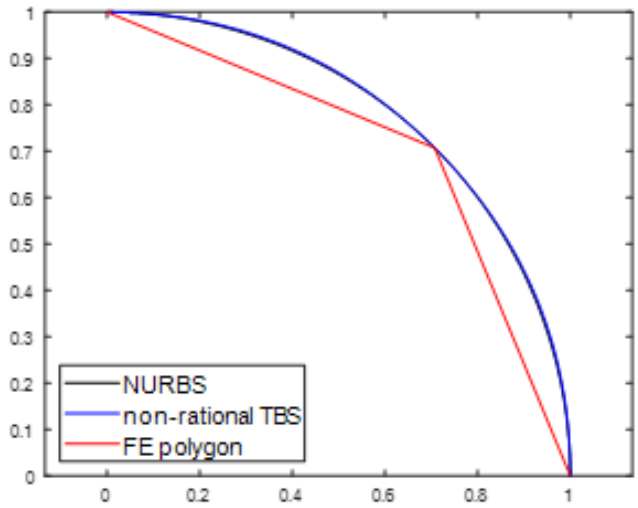

(b) Number of the curves = 2

Fig. 3.5 Comparison of discrepancy respect to the number of the curves

3.3 Macro element split

Although the reconstructed Bezier elements represent the geometry in a reduced geometric discrepancy, the basis function will still be C^0 inter-element continuous. To obtain C^r continuous basis function $(r \geq 1)$, continuity condition should be applied to all the elements. In general, constructing C^1 basis requires one greater than 9th-order tetrahedron. For the computational efficiency, macro element split technique is presented to construct C^1 basis using a lower-order tetrahedron by splitting the original tetrahedron, as shown in Fig. 3.6. After the macro element split, each macro tetrahedron will be split into multiple micro tetrahedron. By doing that, the macro tetrahedron that possess similar number of nodal points as higher-order tetrahedron could be constructed. There are macro element split techniques for construction of C^1 basis formulated, such as Worsey-Piper split utilizing 24 split 2nd-order tetrahedron, Worsey-Farin split using 12 split 3rd-order tetrahedron, and Alfeld split require 5th-order tetrahedron.

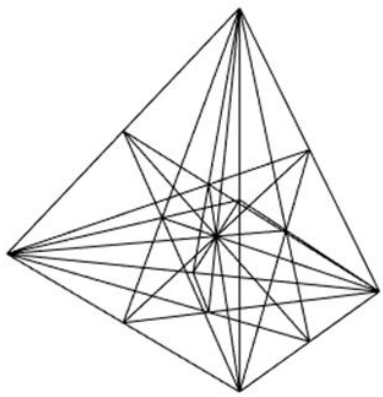

(a) Worsey-Piper split

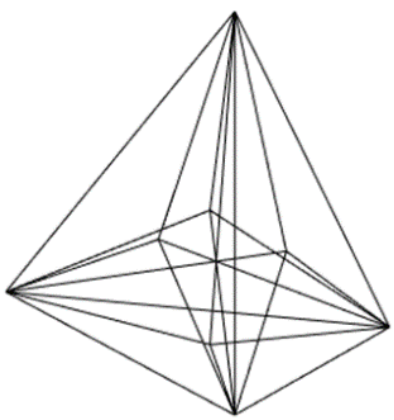

(b) Worsey-Farin split

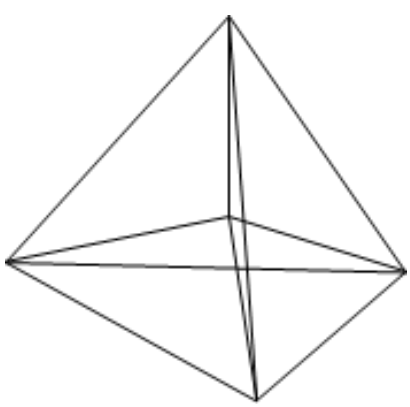

(c) Alfeld split

Fig. 3.6 Macro element split

In this paper, Worsey-Piper split which utilizes a conventional 2nd-order tetrahedral element. Unlike Alfeld split, it requires split condition for each split point as follows:

- Face split point is the intersection point of elemental points that share the same face
- All elemental split point that share an identical edge are on the same plane

The split points are depicted in Fig. 3.7. To fulfill those conditions, the angle of all faces for FE discretized tetrahedron should be an acute. Unfortunately, such constraints are not straightforward to satisfy when it comes to complicated geometry like inner hole-dominant geometry. Therefore, for an alleviation of the geometric constraint the split condition for the edge is disregarded in the present method. Consequently C^1 continuity condition utilizing such macro element split is approximate C^1 continuity condition.

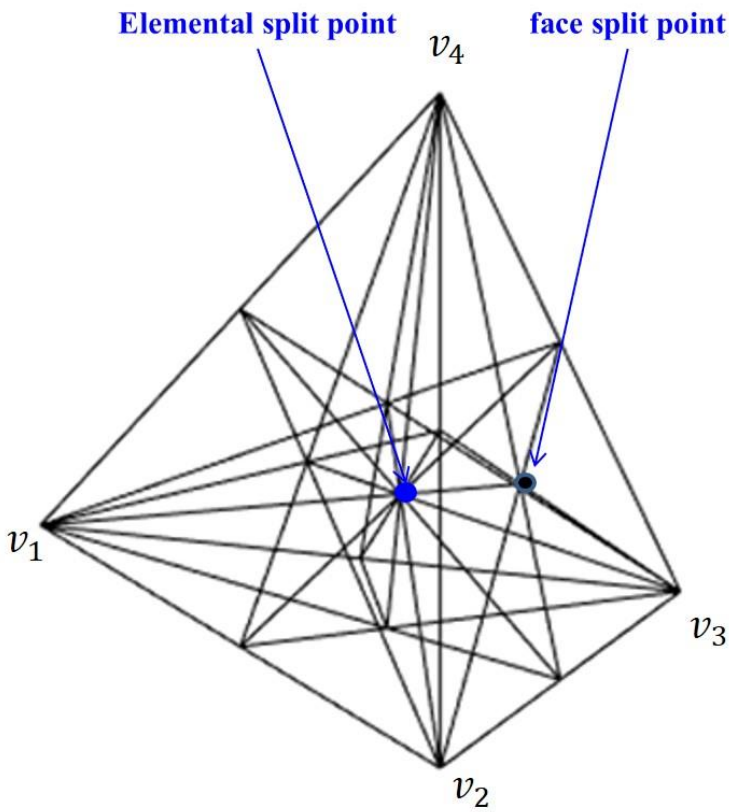

Fig. 3.7 Split points for Worsey-Piper split

3.4 Approximate C^1 Bezier basis function

To construct C^r basis, the continuity condition will be applied for the entire micro tetrahedrons, which is quoted as Hermite interpolation. Hermite interpolation formulation is described as in Eqs. (3.6) - (3.9).

$$\mathbf{s}(\boldsymbol{x_i}, \boldsymbol{y_i}, \boldsymbol{z_i}) = \boldsymbol{k_i} \quad \boldsymbol{for\ i = 1, \dots, n.} \tag{3.6}$$

$$\boldsymbol{D_x}\mathbf{s}(\boldsymbol{x_i}, \boldsymbol{y_i}, \boldsymbol{z_i}) = \boldsymbol{k_i^x} \quad \boldsymbol{for\ i = 1, \dots, n..} \tag{3.7}$$

$$\boldsymbol{D_y}\mathbf{s}(\boldsymbol{x_i}, \boldsymbol{y_i}, \boldsymbol{z_i}) = \boldsymbol{k_i^y} \quad \boldsymbol{for\ i = 1, \dots, n..} \tag{3.8}$$

$$\boldsymbol{D_z}\mathbf{s}(\boldsymbol{x_i}, \boldsymbol{y_i}, \boldsymbol{z_i}) = \boldsymbol{k_i^z} \quad \boldsymbol{for\ i = 1, \dots, n..} \tag{3.9}$$

Where $\mathrm{s}(\boldsymbol{x_i}, \boldsymbol{y_i}, \boldsymbol{z_i})$ is the C^0 Bezier spline at the intersection point. D_xs, D_ys, and D_zs is the x, y, and z direction derivatives of C^0 Bezier spline.

When applying the continuity condition, the directional derivatives of the basis function will be utilized at the interface among tetrahedrons such as a node, edge, and face. By using the Bernstein-Bezier technique, the derivatives of the basis function will be obtained in terms of the barycentric coordinate. After enforcing the continuity condition, there will be some set $\Gamma \subseteq S_d^0(\triangle)$ of the total domain $S_d^0(\triangle)$ that determine all other set in $S_d^0(\triangle)$. Γ is the determining set for S_d^0, and the smallest set of Γ is the minimal determining set (MDS) for S_d^0, and it will be utilized same as the degree of freedom as in the FEM. Figure 3.8 depicts the MDS points for three-dimensional example geometry.

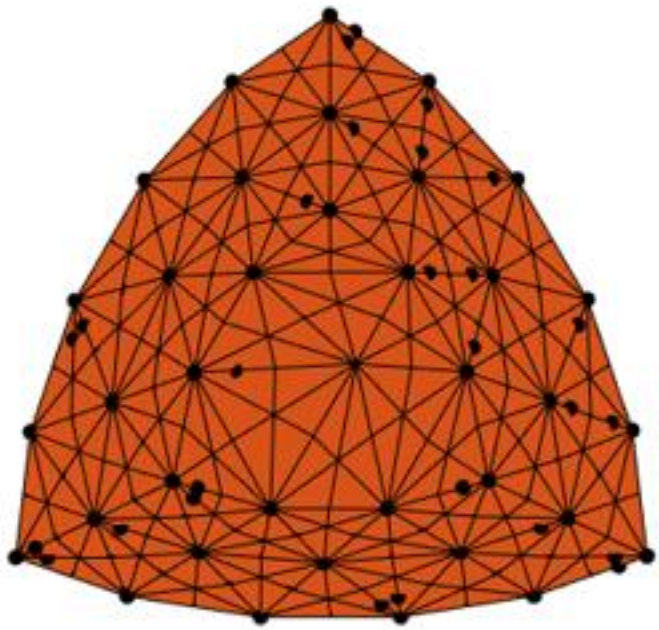

Fig. 3.8 MDS points for the macro element split

As a result of enforcing the continuity condition, all domain points $s \subseteq S_d^0$ is determined as the linear combination of MDS with continuity coefficients as described in Eq. (3.10). The continuity coefficients are obtained from the Hermite interpolation for all intersections of micro tetrahedrons as in Eqs. (3.6) - (3.9).

$$\boldsymbol{c} = \boldsymbol{A}\tilde{\boldsymbol{c}}. \tag{3.10}$$

Where c and $\tilde{c}$ are the all domain points in S_d^0 and MDS points in $\mathcal{M}$, respectively. A is continuity matrix.

Then, the approximate C^1 basis (ψ) at the parametric point ($\hat{\boldsymbol{x}}$) for every tetrahedron T is defined on the MDS ($\mathcal{M}$) by using the C^0 basis (B) at the parametric point ($\hat{\boldsymbol{x}}$) and continuity coefficients (a), of which component for continuity matrix (A) as described in Eq. (3.11).

$$\boldsymbol{\psi}_{\xi|T}(\hat{\boldsymbol{x}}) = \sum_{\boldsymbol{\eta} \in \boldsymbol{D}_{d,T}} \boldsymbol{a}_{\eta\xi}\, \boldsymbol{B}_{\boldsymbol{\eta}}^{\boldsymbol{T}}(\hat{\boldsymbol{x}}). \tag{3.11}$$

Where ξ and η are the point of the set of MDS ($\mathcal{M}$) and the set of domain points ($D_{d,T}$), respectively. $a_{\eta\xi}$ is the component of η-th column, ξ-th low of the continuity matrix A.

The constructed approximate C^1 basis is unity for each $\xi \in \mathcal{M}$ as described in Eq. (3.11). Because the continuity coefficient for the MDS point is only unity on the corresponding points, and all other components is zero.

$$\boldsymbol{\gamma}_{\boldsymbol{\eta}}\boldsymbol{\psi}_{\xi} = \boldsymbol{\delta}_{\boldsymbol{\eta},\xi}, \quad \boldsymbol{for}\ \boldsymbol{\eta} \in \boldsymbol{\mathcal{M}}. \tag{3.12}$$

Where γ_η is the linear functional such that for every $s \in S_d^0$, $\gamma_\eta s$ is the Bezier

coefficient of s corresponding to the domain point η. δ is the direc delta function.

Because the constructed approximate C^1 basis satisfy the condition for shape function on the MDS, it can be used in traditional FE formulation easily. It will be verified in the next section by applying this for numerical analysis.

Chpater 4

Numerical results

4.1 Formulation

As described in the previous chapter, the approximate C^1 basis can be utilized in traditional FE formulation easily. Therefore, formulation of the present method is identical except the approximation is conducted on MDS. By utilizing that formulation, linear static structural analysis using TBS-based IGA is carried out for the curved solid objects including turbine blade geometry. First, the present method is applied to the example geometries which the analytic solution exists [23]. That includes Infinite plate with 3D hole, Spherical cavity in an infinite solid, and Inner pressurized hollow sphere. To verify that the present method obtains more precise result than traditional FEM does, comparison of those results against the analytic solution will be conducted by using the same meshes. Furthermore, improved applicability of the present method is demonstrated by applying it for NASA Rotor 67 blade.

The governing equation, boundary condition and physical displacement approximation are conducted only on MDS as described in Eqs. (4.1) – (4.4). Moreover, stiffness matrix constructed by using only MDS as described in Eq. (4.5).

$$\boldsymbol{\nabla} \cdot \boldsymbol{\sigma} + \boldsymbol{b_f} = \mathbf{0} \quad \boldsymbol{on}\ \boldsymbol{\Omega}. \tag{4.1}$$

$$\boldsymbol{\sigma} \cdot \boldsymbol{n} = \boldsymbol{t} \quad \boldsymbol{on}\ \boldsymbol{\Gamma_t}. \tag{4.2}$$

$$\boldsymbol{u} = \overline{\boldsymbol{u}} \quad \boldsymbol{on}\ \boldsymbol{\Gamma_u}. \tag{4.3}$$

$$\boldsymbol{S} = \sum_{\xi \in \mathcal{M}} \boldsymbol{c_\xi \psi_\xi} = \sum_{\xi \in \mathcal{M}_b} \boldsymbol{c_\xi \psi_\xi} + \sum_{\xi \in \mathcal{M}_0} \boldsymbol{c_\xi \phi_\xi}\,. \tag{4.4}$$

$$\boldsymbol{K_{MDS}} = [\boldsymbol{A}]^{\boldsymbol{T}}[\boldsymbol{K}][\boldsymbol{A}]. \tag{4.5}$$

Where Ω is the total domain. Γ_t and Γ_u are the surface imposed by the Neumann and Dirichlet boundary condition, respectively. c_ξ and S are the Bezier control variable and Bezier approximation, respectively. $\mathcal{M}$, $\mathcal{M}_0$, and $\mathcal{M}_b$ is the set of MDS pints, the list belonged to both the set of MDS points and Γ_t, and the list of MDS points except the points in $\mathcal{M}_0$, respectively.

4.2 Numerical result

4.2.1 Infinite plate with a three-dimensional hole

As a first numerical example for verification of the present method, Infinite plate with 3D hole with radius a = 0.25m, length of plate L = 1m, and thickness of plate t = 0.25m. The plate with Young's modulus E = 1000 Pa and Poisson's ratio υ = 0.3, subjected to a uni-directional tensile load $T_{inf} = 1$ Pa which applied at an infinite distance from the three-dimensional hole will be selected as shown in Fig. 4.1. For reducing the expense of the analysis, the quarter of the geometry will be considered, and symmetry boundary condition be imposed on the planar surfaces which are perpendicular to x and y direction. The object is selected by the reason that stress concentration at the curved surface, and it is the one of the conventional examples for verification of the numerical solution.

The pre-processing method is conducted as shown in Fig. 4.2. For the verification of the present method, the analysis by the present method and traditional FEM both are conducted on the identical discretization. The discrepancy against the analytic solution [23] of both method are measured by $H^0 - norm\ error$, $\|e_\sigma\|_{H^0}$, [23] as expressed in Eq. (4.6).

$$\|\boldsymbol{e_\sigma}\|_{\boldsymbol{H^0}} = \sqrt{\sum_{\boldsymbol{m=1}}^{\boldsymbol{nel}} \left(\frac{\int (\boldsymbol{\sigma_{ex}} - \boldsymbol{\sigma_g^m}) \cdot (\boldsymbol{\sigma_{ex}} - \boldsymbol{\sigma_g^m})\, \boldsymbol{dV}}{\int \boldsymbol{\sigma_{ex}} \cdot \boldsymbol{\sigma_{ex}}\, \boldsymbol{dV}} \right)} \tag{4.6}$$

Where σ_{ex} and σ_g are the analytic von-Mises stress at gauss point and numerically calculated von-Mises stress at gauss point, respectively. nel is the number of

elements.

The comparison of the discrepancy in von-Mises stress of the present method with traditional FEM for the mesh refinement is illustrated in Fig. 4.3. The convergence curve in Fig. 4.3 visualizes the improved accuracy of the present method in terms of the mesh refinement.

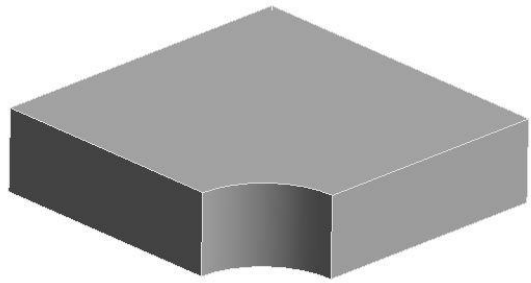

(a) three-dimensional geometry

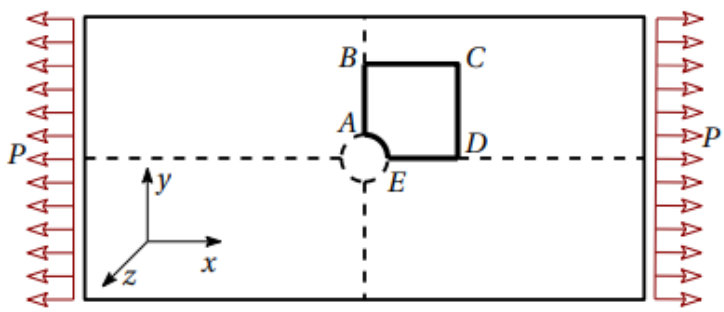

(b) Conventional two-dimensional example [23]

Fig. 4.1 Infinite plate with a three-dimensional hole

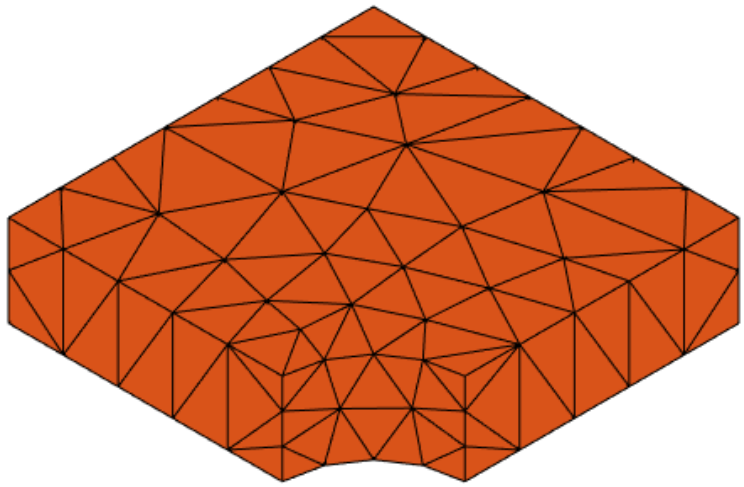

(a) FE discretization

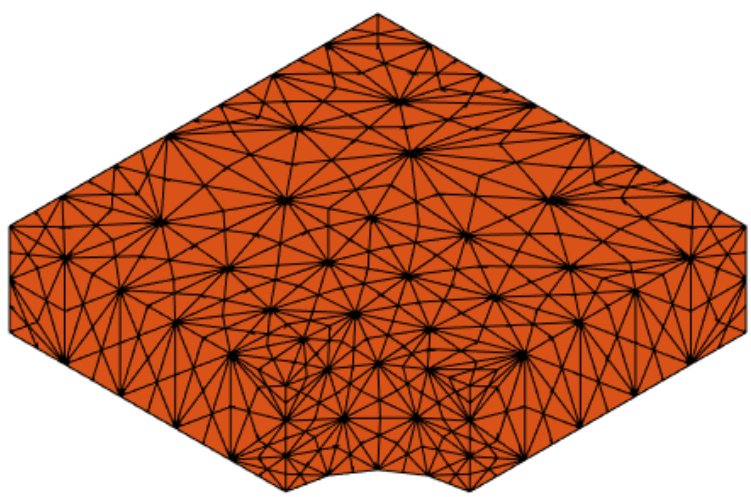

(b) Macro element split

Fig. 4.2 Pre-processing for TBS-based IGA

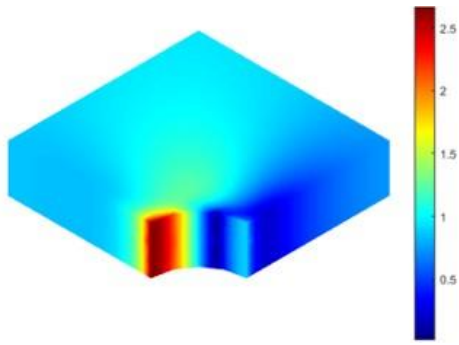

(a) Analytic solution for von-Mises stress

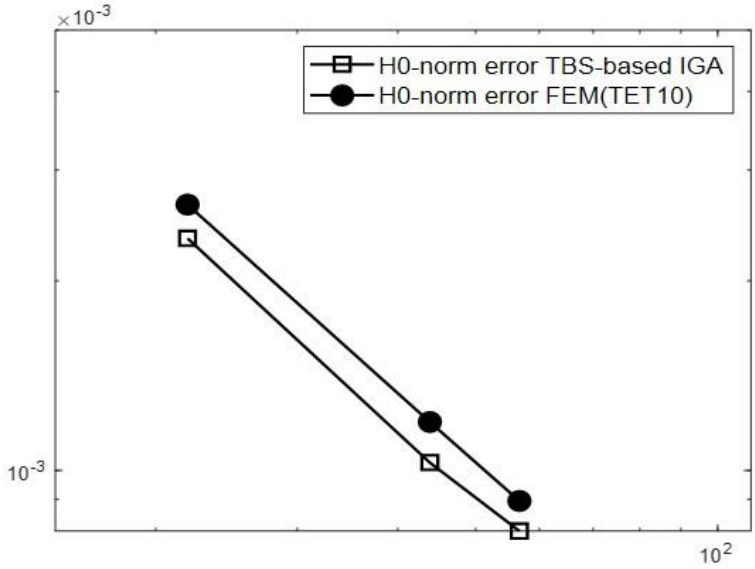

(b) Convergence curve of von-Mises stress

Fig. 4.3 Comparison of Numerical solution

4.2.2 Spherical cavity in an infinite solid

As a second numerical example for verification of the present method, Spherical cavity in an infinite solid with radius a = 0.1m, length of solid L = 0.4m with Young's modulus E = 1,000 Pa and Poisson's ratio υ = 0.3, subjected to a uni-directional tensile load $T_{inf} = 1$ Pa which applied at an infinite distance from the cavity will be selected as shown in Fig. 4.4. For reducing the expense of the analysis, the eighth of the geometry will be considered, and symmetry boundary condition be imposed on the planar surfaces which are perpendicular to x, y, and z direction. In figure. 4.5, the pre-processing for TBS-based IGA is described.

The comparison on von-Mises stress between the present method and the traditional FEM for the mesh refinement is illustrated in Fig. 4.6. The convergence curve depicted in Fig. 4.6 visualizes the improved accuracy of the present method in terms of the mesh refinement. In the convergence curve, Although the difference of discrepancy is small, the convergence rate along the mesh refinement is larger in the present method than the traditional FEM.

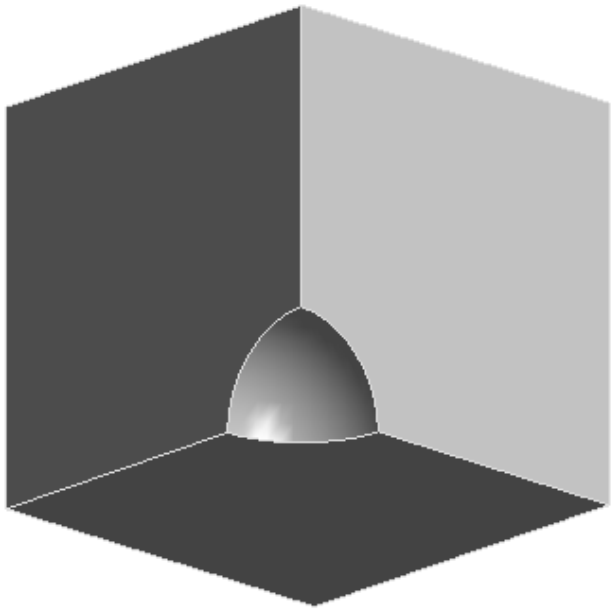

Fig. 4.4 Configuration of the example

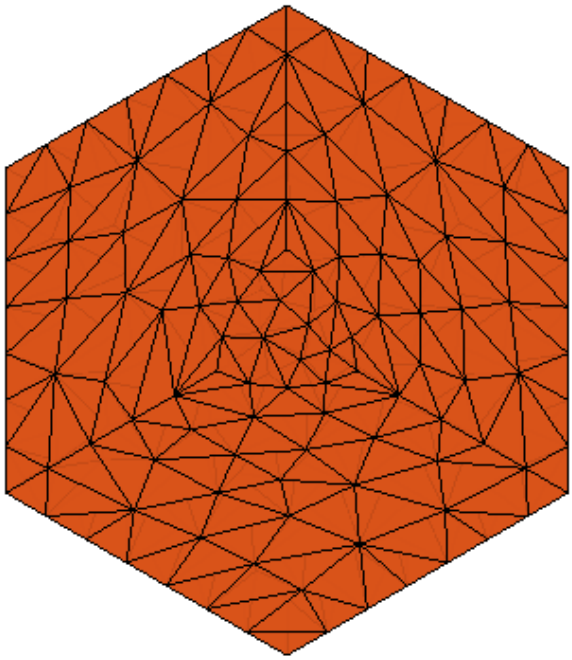

(a) FE discretization

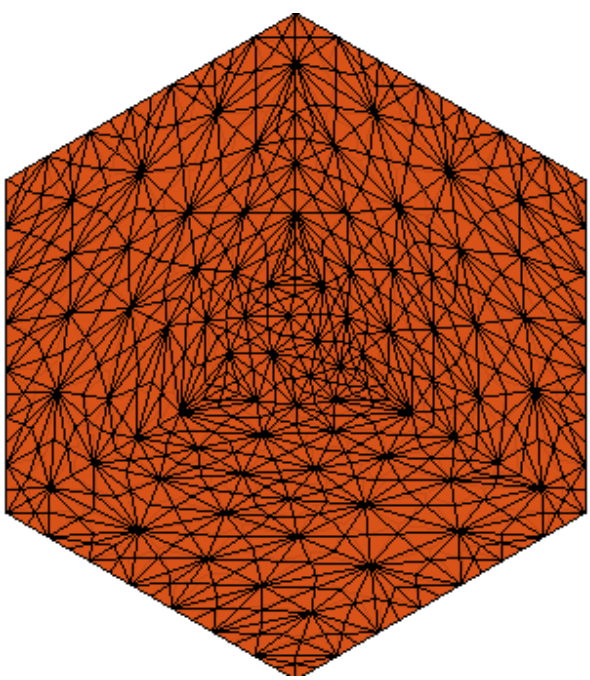

(b) Macro element split

Fig. 4.5 Pre-processing for TBS-based IGA

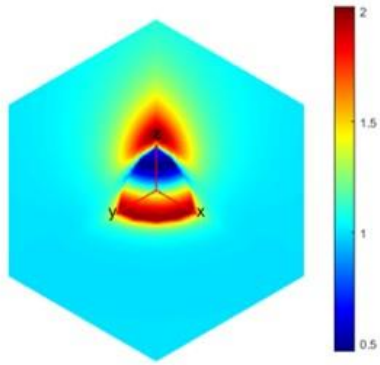

(a) Analytic solution for von-Mises stress

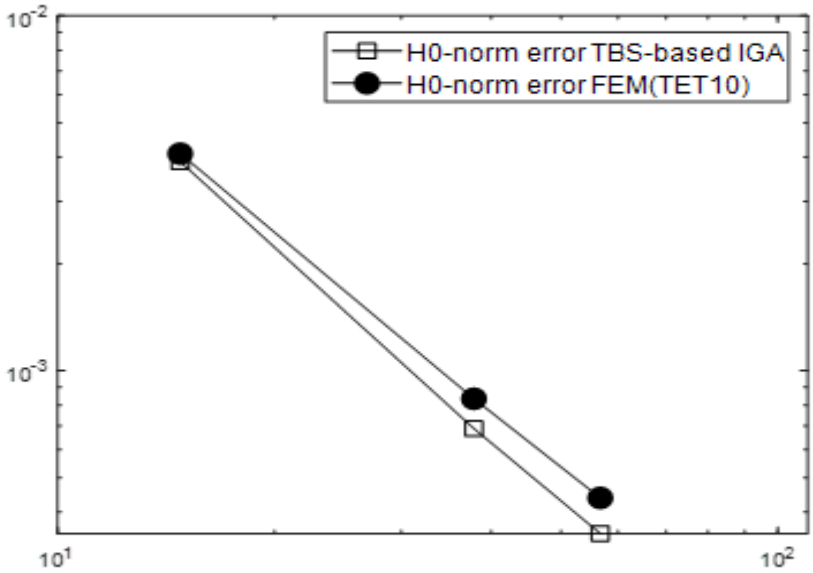

(b) Convergence curve of von-Mises stress

Fig. 4.6 Comparison of the result

4.2.3 Inner pressurized hollow sphere

As a final numerical example for verification of the present method, a hollow sphere with inner radius a = 0.5m and outer radius b = 1m, subjected to a uniform internal pressure p = 1Pa will be selected as shown in Fig. 4.7. For reducing the expense of the analysis, an eight part will be considered as in previous example. Also, same symmetry boundary condition will be imposed. The reasons for the selection of the object are the stress concentration on the curved surface and curvature that increases toward the inside from the exterior. Moreover, such object is constructed mostly with curved surface when compared with the previous objects.

(a) Analysis geometry

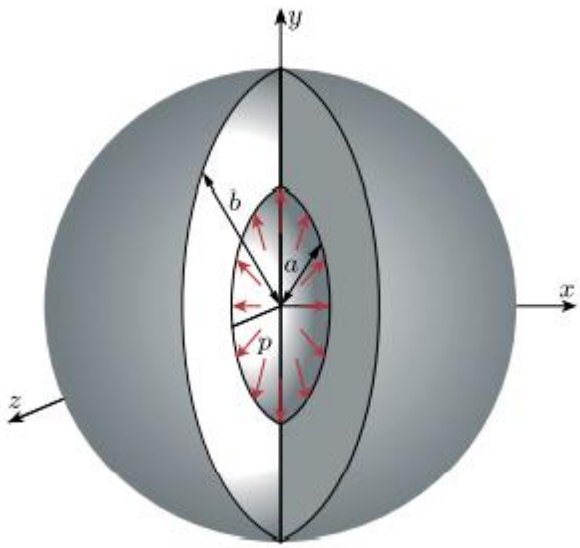

(b) Hollow sphere []

Fig. 4.7 Configuration of the example

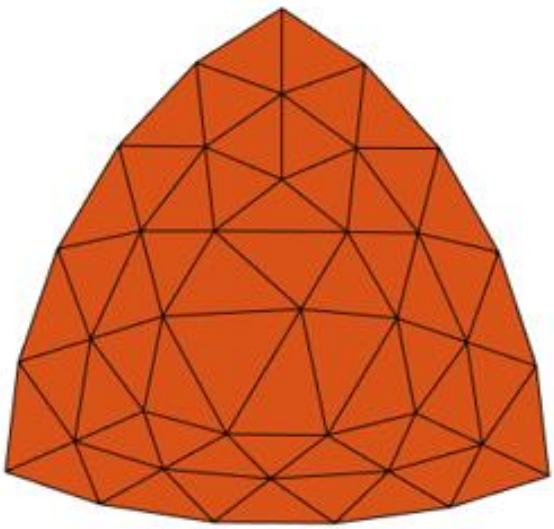

(a) FE discretization

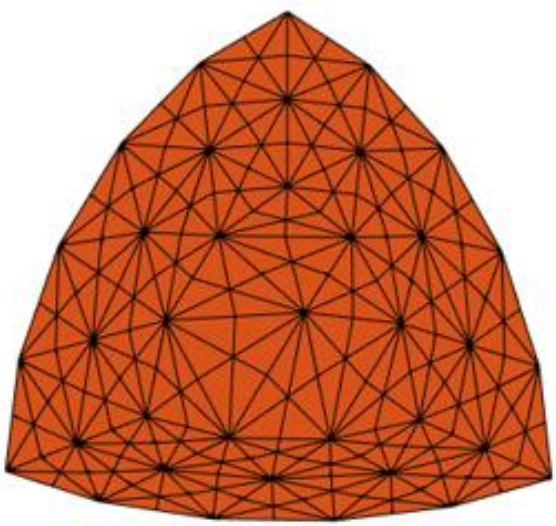

(b) Macro element split

Fig. 4.8 Pre-processing for TBS-based IGA

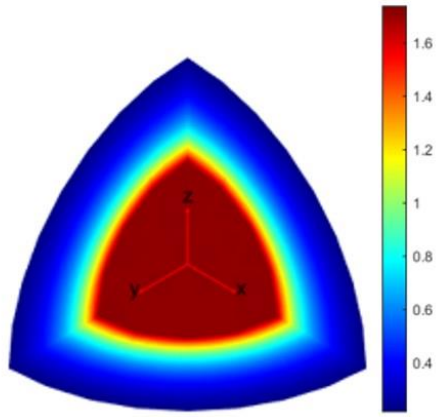

(a) Analytic solution for von-Mises stress

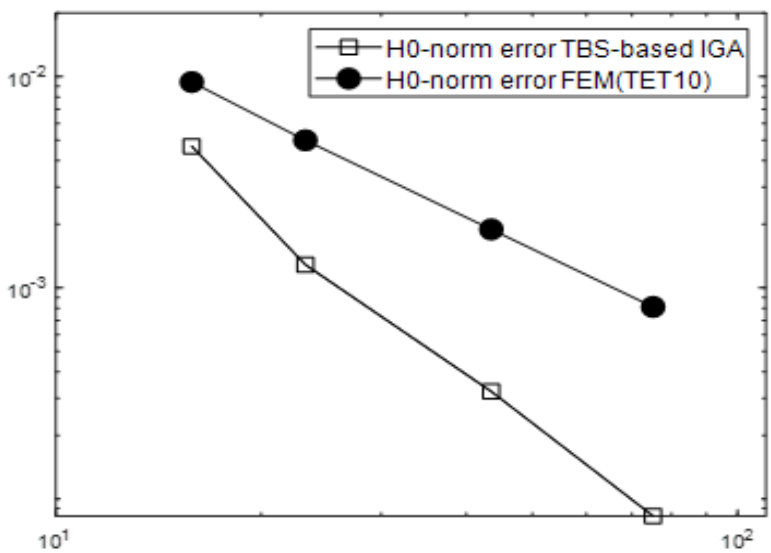

(b) Convergence curve of von-Mises stress

Fig. 4.9 Comparison of the result

For the verification of the present TBS-based IGA, three examples which exists an analytic solution are selected, and the discrepancy of von-Mises stress obtained from the present method and traditional FEM.

When the results of convergence curve are compared, the discrepancy of the present method is much lower than traditional FEM on the 3rd example. The reasons for that result will be the boundary condition which applied on curved surface and the 3rd object is constructed mostly with curved geometry.

From the results of the three examples for verification, it is confirmed that the present method provides more precise numerical solution. Furthermore, such advantage will be maximized for analysis of the curve-dominant configuration.

Industrial geometries in mechanical, aerospace, and naval engineering are mostly constructed of curved geometry for improved efficiency. Therefore, the present method will be helpful for predicting the precise numerical solution for such configuration.

Table. 4.1 Mesh information of the present analysis

Type	No. of macro nodes	No. of micro nodes	No. of MDS nodes
Case 1	330	5,977	240
Case 2	940	18,411	620
Case 3	5,507	117,477	3,276
Case 4	27,073	598,213	13,272

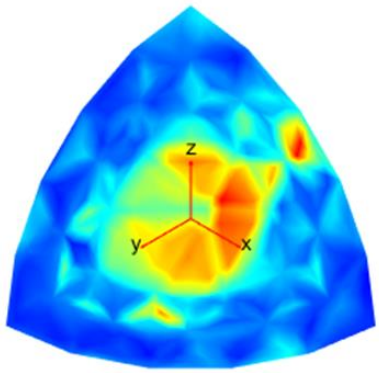

(a) TBS-based IGA

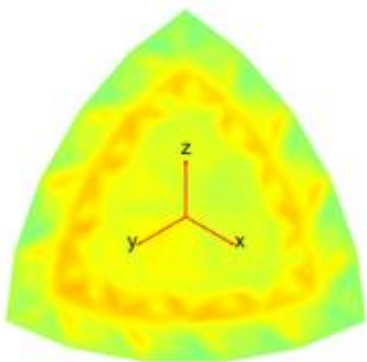

(b) FEM (TET10)

Fig. 4.10 von-Mises stress discrepancy distribution for Case 1

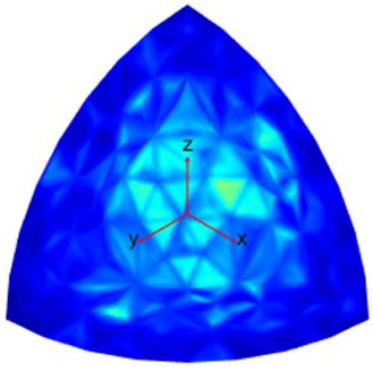

(a) TBS-based IGA

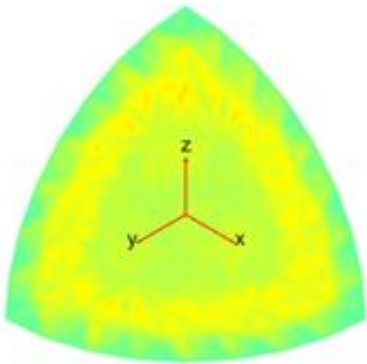

(b) FEM (TET10)

Fig. 4.11 von-Mises stress discrepancy distribution for Case 2

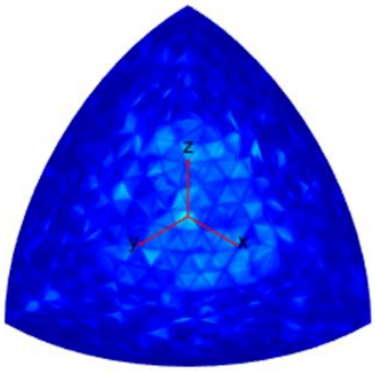

(a) TBS-based IGA

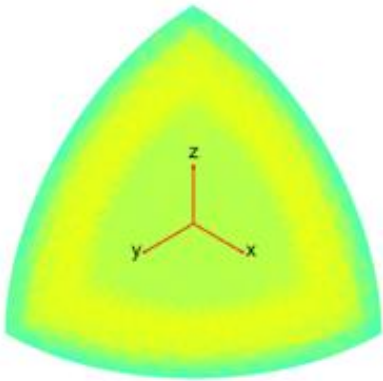

(b) FEM (TET10)

Fig. 4.12 von-Mises stress discrepancy distribution for Case 3

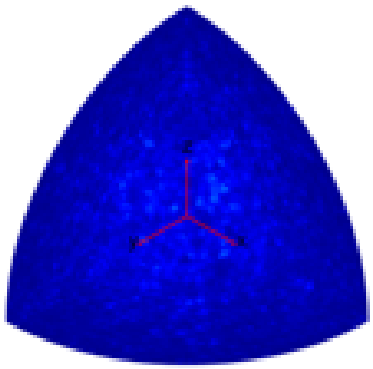

(a) TBS-based IGA

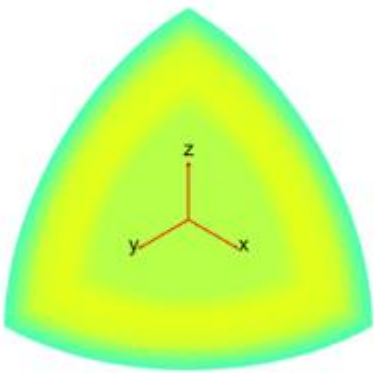

(b) FEM (TET10)

Fig. 4.13 von-Mises stress discrepancy distribution for Case 4

4.2.4 NASA Rotor 67

As a numerical application for indication of improved applicability, a single blade of NASA Rotor 67 with tip load f=600N and fixed condition of a root of the blade is selected as shown in Fig. 4.14. By utilizing commercial FEM software with a conventional 2nd-order tetrahedron for FE discretization and unification of all the other pre-processing in the present in-house code, the present method has improved applicability for arbitrary solid object as shown in Fig. 4.15.

Figure 4.16 illustrate the von-Mises stress distribution obtained from the present method, and the maximum stress is observed on the thinnest location of the blade.

(a) single blade

(b) Entire packet

Fig. 4.14 Configuration of the example

(a) Force condition

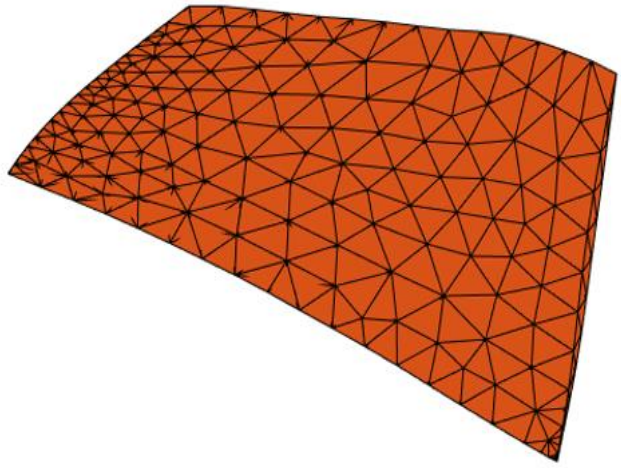

(b) FE discretization

Fig. 4.15 Configuration of the example

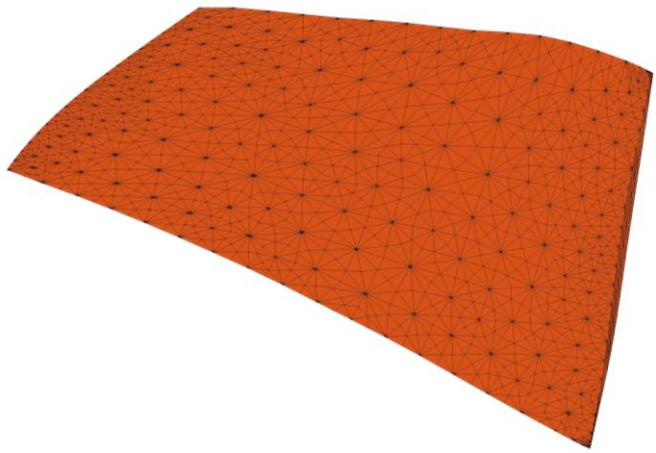

(a) Macro element split

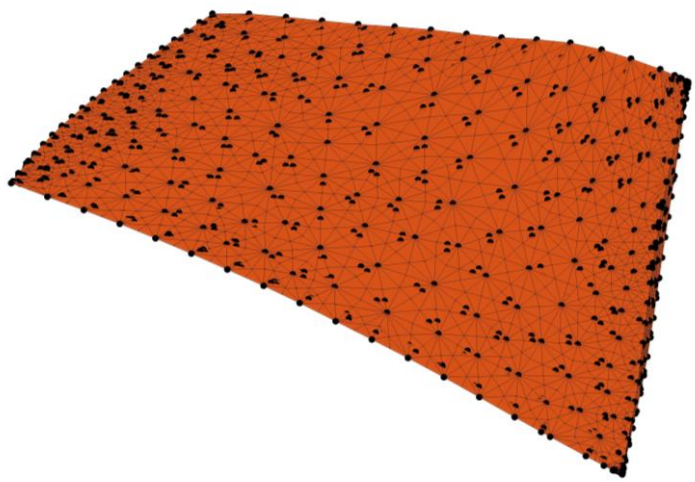

(b) MDS

Fig. 4.16 Configuration of the pre-processing

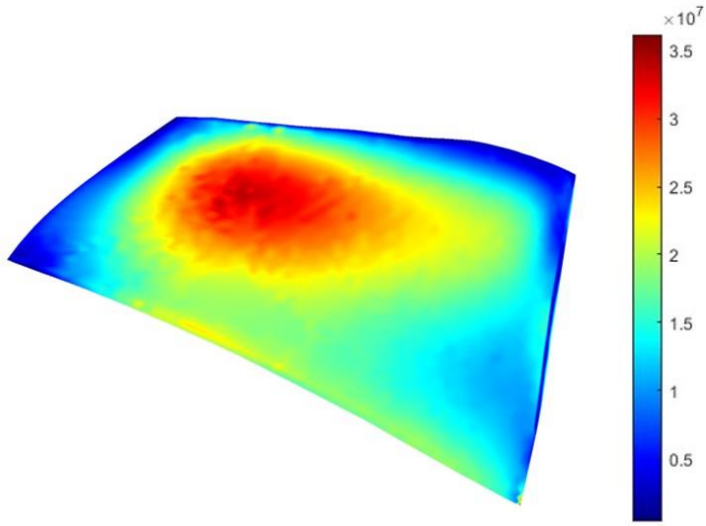

Fig. 4.17 von-Mises stress distribution from the present method

Chapter 5

Conclusion and Future works

5.1 Conclusion

In this thesis, TBS-based IGA by using Benrstein-Bezier discretization is attempted for the structural analysis of the curved solid object including a turbine blade. In NURBS-based IGA, by utilizing the shape function as NURBS basis that used for geometry representation in CAD, more accurate numerical solution can be calculated than traditional FEM. The main features of that advantage are the geometric exactness and high-continuity of the basis function.

Because there is no suitable preprocessor for NURBS-based IGA, applying IGA to a three-dimensional solid object for more precise analysis has been a challenge in the field. The main reasons of that are the NURBS defined as tensor product, and the B-rep of the general CAD software. To solve such limitation, many alternatives have been proposed including the method using the 5th order Bezier tetrahedral element. The present method is one of such efforts, and inspired from the previous work.

The present method utilizes FE discretization for inner volumetric parameterization, and some pre-processing is conducted to implement the features of NURBS-based IGA. From the FE discretized geometry, surface reconstruction is conducted to reduce the geometric discrepancy that occurred on the curved surface between the CAD geometry and the FE polygon. After that, for the high continuity

of the basis function, the additional continuity condition is applied. In the process, the macro element split technique is used for computational efficiency in the entire analysis.

Because the present approach requires the discretization information of the commercial FEM software only, it will exhibit improved applicability for an arbitrary complicated solid object than the other alternatives do based on the complex NURBS information. An approximate C^1 Bezier basis function is constructed by violating the split condition of macro edge for alleviation of geometric constraint.

For the verification of the present method, three-dimensional curved solid objects are selected. The analysis is conducted on the same mesh for the present method and traditional FEM. Calculation of the discrepancy is conducted the $H^0 - norm$ error with the analytic solution. Form the convergence curve of discrepancy for all example geometry that compared, the discrepancy in von-Mises stress is found to be superior in the prediction by the present method than that by the traditional FEM for an entirely refined mesh set. Especially, the discrepancy in the 'Inner pressurized hollow sphere' is much smaller than that of FEM compared to the other example. The first reason of that is the boundary condition applied on the curved surface. Because the boundary condition is applied on the physical point unlikely in the FEM that applied on the FE node. The second reason is the portion of the curved surface in the entire configuration. That geometry is mostly constructed using curved surfaces. Therefore, the effect of surface reconstruction will be larger than the other

examples. After the verification for the precise numerical analysis of the present method, to verify the improved applicability of the present method to an arbitrary solid object NASA Rotor 67 blade is selected. By applying the same pre-processing as in the example geometry, it shows that the present method can be applied to arbitrary solid geometry easily.

5.2 Recommendation for the Future works

The followings are suggested for the future tasks for extending the present in-house analysis to conduct a more realistic numerical simulation.

- Application of the present method for the other industrial geometries including the inner hole-dominant configuration.

- Extension of the present method from the linear static analysis to nonlinear and dynamic analysis for more realistic numerical analysis.

- Parametric space optimization for the optimal convergence.

References

[1] Hughes, T. J. R., Cottrell, J. A., and Bazileves, Y., "Isogeometric analysis: CAD, finite elements, NURBS, exact geometry and mesh refinement," *Computer Methods in Applied Mechanics and Engineering*, Vol. 194, No. 39-41, 2005, pp. 4135, 4195.

[2] Cottrell, J. A., Reali, A., Bazileves, Y., and Hughes, T. J. R., "Isogeometric analysis of structural vibrations," *Computer Methods in Applied Mechanics and Engineering*, Vol. 195, No. 41-43, 2006, pp. 5257, 5296

[3] Hughes, T. J. R., Reali, A., and Sangalli, G., "Duality and unified analysis of discrete approximations in structural dynamics and wave propagation: Comparison of p-method finite elements with k-method NURBS," *Computer Methods in Applied Mechanics and Engineering*, Vol. 197, No. 49-50, 2008, pp. 4104, 4124.

[4] Gomez, H., Hughes, T. J. R., Nogueira, X., and Calo, V. M., "Isogeometric analysis of the isothermal Navier-Stokes-Korteweg equations," *Computer Methods in Applied Mechanics and Engineering*, Vol. 199, No.25-28, 2010, pp. 1828, 1840.

[5] Buffa, A., Sangalli, G., and Vanquez, R., "Isogeometric analysis in electromagnetics: B-spline approzimation," *Computer Methods in Applied Mechanics and Engineering*, Vol. 199, No.17-20, 2010, pp. 1143, 1152.

[6] Benson, D. J., Bazileves, Y., Hsu, M. C., and Hughes, T. J. R., "Isogeometric shell analysis:The Reissner-Mindlin shell," *Computer Methods in Applied Mechanics and Engineering*, Vol. 199, No.5-8, 2010, pp. 276, 289.

[7] Bazileves, Y., Hsu, M. C., and Scott, M. A., "Isogeometric fluid-structure interaction analysis with emphasis on non-matching discretizations, and with application to wind turbines," *Computer Methods in Applied Mechanics and Engineering*, Vol. 249-252, 2012, pp. 28, 41.

[8] Aigner, M., Heinrich, C., Juttler, B., Pilgerstorfer, E., Simeon, B., and Vuong, A.-V., "Swept Volume Parameterization for Isogeometric Analysis," *Computer Methods in Applied Mechanics and Engineering*, Vol. 5654, 2009, pp. 19-+.

[9] Kim, H. J., Seo, Y. D. and Youn, S. K.., "Isogeometric analysis for trimmed CAD surfaces," *Computer Methods in Applied Mechanics and Engineering*, Vol. 198, No. 37-40 2012, pp. 2982, 2995.

[10] Jaxon, N., and Qian, X., "Isogeometric analysis on triangulations," *Computer-Aided Design*, Vol. 46, 2014, pp. 45-57.

[11] Xia, S., and Qian, X., "Isogeometric analysis with Bezier tetrahedra," *Computer Methods in Applied Mechanics and Engineering*, Vol. 316, 2017, pp. 782-816.

[12] Kadapa, C., "Novel quadratic Bezier triangular and tetrahedral elements using existing mesh generators: Applications to linear nearly incompressible elastostatics and implicit and explicit elastodynamics," *International Journal for Numerical Methods in Engineering*, Vol. 117, No. 5, 2018, pp. 543-573.

[13] Bazileves, Y., Calo, V. M., Cottrell, J. A., Evans, J. A., Hughes, T. J. R., Lipton, S., Scott, M. A., and Sederberg, T. W., "Isogeometric analysis using T-splines," *Mathematics of Surfaces*, Vol. 199, No.5-8, 2010, pp. 229, 263.

[14] Whetten, C., Sederberg, M., Scott, M., "Isogeometric analysis using the IGA_INCLUDE_BEZIER keyword in LS-DYNA," *European LS-DYNA Conference,* Koblenz, 2019

[15] Chasapi, M., Mester., L., Simeon., B., and Klinkel., S., "Isogeometric analysis of 3D solids in boundary representation for problems in nonlinear solid mechanics and structural dynamics," *International Journal for Numerical Methods in Engineering*, Vol. 123, No. 5, 2022, pp. 1228-1252.

[16] Grossmann, D., Juttler, B., Schlusnus, H., Barner, J., and Vuong, A. V., "Isogeometric simulation of turbine blades for aircraft engines," *Computer Aided Geometric Design*, Vol. 29, No.7, 2012, pp. 519, 531.

[17] Hsu, M. C., Wang, C. L., Herrema, A. J., Schillinger, D., Ghoshal, A., and Bazilevs, Y., "An interactive geometry modeling and parametric design platform for isogeometric analysis," *Computers and Mathematics with Application*, Vol. 70, No. 7, 2015, pp. 1481-1500.

[18] Bazilievs, Y., Takizawa, K., Wu, M. C. H., Kuraishi, T., Avsar, R., Xu, Z. J., and Tezduyar, T. E., "Gas turbine computational flow and structure analysis with isogeometric discretization and a complex-geometry mesh generation method," *Computational Mechanics,* Vol. 67, No. 1, 2021, pp. 57-84.

[19] Lai, M. J., and Schumaker, L. L., *Spline Functions on Triangulations*, Vol. 110., Cambridge university press, Cambridge, 2007, Chaps. 5-18

[20] Borden, M. J., Scott, M. A., Evans, J. A., and Hughes, T. J. R., "Isogeometric finite element data structures based on Bezier extraction of NURBS," *International Journal for Numerical Methods in Engineering,* Vol. 87, No. 1-5, 2011, pp. 15-47.

[21] Thomas, D. C., Scott, M. A., Evans, J. A., Tew, K., and Evans, E. J., "Bezier Projection: a unified approach for local projection and quadrature-free refinement and coarsening of NURBS and T-splines with particular application to isogeometric design and analysis," *Computer Methods in Applied Mechanics and Engineering*, Vol. 367, 2020, 113066.

[22] Piegl, L., and Tiller, W., *The NURBS book*, 2nd ed., Springer Science & Business Media, Berlin, 2012, Chaps. 2-12

[23] Sharma, R., Zhang., J., Langelaar., M., Keulen., F., and Aragon., A., "An improved stress recovery technique for low-order 3D finite elements," *International Journal for Numerical Methods in Engineering*, Vol. 114, No. 1, 2018, pp. 88-103.

[24] Payen, D. J., and Bathe., K. J., "A stress improvement procedure," *Computers & Structures*, Vol. 112-113, 2012, pp. 311-326.

[25] Schumaker, L. L., *Spline Functions: Computational methods*, Society for industrial and Applied Mathematics, Philadelpia, 2015, Chaps. 4-9

[26] Kang, S. H., K, Y. S., Cho, H, S., and Shin, S, J., "Improved hyper-reduction

approach for the forced vibration analysis of rotating components," *Computational Mechanics,* Vol. 69, 2022,pp. 1443-1456.

[28] Matt, M, A., *Trivariate Local Lagrange interpolation and Macro elements of Arbitrary Smmoothness..*, Springer Science & Business Media, Berlin, 2012, Chaps. 1-5

국문초록

고정밀 구조응답 예측을 위한 Bezier 사면체 요소 기반 isogeometric 해석 개발

송동현

서울대학교 대학원

항공우주공학과

본 논문에서는 고정밀 구조해석을 위한 유한요소 이산화 기반 TBS-기반 아이소-지오메트릭 해석 프레임워크를 구축하였다. 기존의 유한요소해석에서는 해석을 위해 유한요소 이산화 과정이 필수적이며, 복잡한 형상에 대한 이산화 과정에서 CAD 형상과의 기하학적 오차가 발생한다. 반면, isogeometric 해석은 CAD 에서 사용되는 형상표현법을 활용하여 기존 FEM 보다 정밀한 해석을 도출하는 것이 입증되어 왔다. 가장 큰 원인으로는 CAD 와 같은 형상표현을 통한 형상의 정확성과 NURBS 기저함수의 요소간 높은 연속성이다. 하지만, 일반적으로 CAD 프로그램에서 3 차원 솔리드 형상을 표현할 때, 형상의 내부를 제외하고 겉부분만을 표현하기 때문에 이를 해석에 이용하기에 어려움이 있다. 이 같은 한계를 극복하기 위해 많은 대안들이 제시되어 왔으며 본 논문은 5 차 Bezier 사면체 요소를 활용하는 대안에서

영감을 얻었다.

본 논문에서 소개된 Bezier 사면체 요소 기반 isogeometric 해석 프레임워크는 다음과 같다. 먼저, 상용 유한요소 프로그램을 통해 겉부분만 표현된 CAD 형상을 내부까지 이산화하고, 기하학적 오차 감소를 위해 이산화된 유한요소 다각형을 Bezier 요소로 변환한다. 이후 높은 요소 간 연속성 획득을 위해 추가의 연속 조건을 적용하며, 이 과정에서 높은 적용성을 위해 근사 C^1 기저함수를 구성하며, 이후 진행되는 해석 과정에서 이를 활용한다.

이와 같이 구성된 전체 프레임워크를 이론해가 존재하는 곡면을 포함하는 예제 형상에 적용하고 이를 동일한 유한요소 이산화에서 본 기법, FEM 의 결과를 이론해와 비교한 오차의 수렴도 곡선을 통해 본 기법의 타당성을 증명하였다. 또한, 본 기법의 높은 기하학적 적용성의 입증을 위해 임의의 솔리드 형상인 NASA Rotor 67 에 적용하였다.

주제어: 아이소-지오메트릭 해석, 유한요소법, 사면체 Bezier 곡선 기저함수, 거시적 요소 분할, 연속 조건 , 유한요소 이산화,

학번: 2021-27453